

Monochromatic and random wave breaking at blocking points

Arun Chawla

Center for Coastal and Land-Margin Research, Department of Environmental Science and Engineering, Oregon Graduate Institute of Science and Technology, Portland, Oregon, USA

James T. Kirby

Center for Applied Coastal Research, University of Delaware, Newark, Delaware, USA

Received 26 June 2001; revised 18 December 2001; accepted 27 December 2001; published 4 July 2002.

[1] In this paper we study the energy dissipation due to current-limited wave breaking in monochromatic and random waves with the help of experimental tests. The opposing currents are strong enough for wave blocking to occur. A modified bore model is used to simulate the dissipation rate in the monochromatic waves, and an empirical bulk dissipation formula for wave breaking in random waves is proposed. The effects of wave blocking on the dynamics of the wave field are also discussed. *INDEX TERMS:* 4546

Oceanography: Physical: Nearshore processes; 4560 Oceanography: Physical: Surface waves and tides (1255); 4512 Oceanography: Physical: Currents; 4528 Oceanography: Physical: Fronts and jets; *KEYWORDS:* wave-current interaction, wave breaking, wave action conservation, nonlinear dispersion, inlets

1. Introduction

[2] Wave blocking is the phenomenon by which propagating waves are stopped by strong opposing currents. As waves propagate into opposing currents, their group velocity reduces, leading to an increase in wave height. If the current is strong enough, then the group velocity could go to zero, causing the waves to become blocked. This is a fairly common phenomenon at the entrances of tidal inlets where tidal currents can become very strong. One such example of wave blocking is shown in Figure 1, where the view is looking seaward from the southern inlet breakwater. The photograph has been taken 3 hours after high tide, and thus there is a strong current propagating out of the inlet. This strong current blocks waves that are trying to propagate into the inlet. Owing to the sharp increase in wave steepness prior to blocking, the wave environment tends to become very rough, as can be seen in Figure 2. This causes considerable navigational hazard, and boats have been known to capsize trying to cross inlets under such circumstances.

[3] For a two-dimensional wave moving on a depth uniform current given by the velocity vector \mathbf{U} , the dispersion relation for a monochromatic wave is given by

$$\omega - \mathbf{k} \cdot \mathbf{U} = \sigma, \quad (1)$$

where ω is the absolute frequency relative to a stationary observer, \mathbf{k} is the wave number vector, and σ is the intrinsic wave frequency, or frequency relative to an observer moving at velocity \mathbf{U} . Differentiating equation (1) with respect to \mathbf{k} gives

$$\mathbf{C}_{ga} - \mathbf{U} = \mathbf{C}_g, \quad (2)$$

where $\mathbf{C}_{ga} = \partial\omega/\partial\mathbf{k}(\mathbf{k}/k)$ is the vector group velocity in a stationary frame and $\mathbf{C}_g = \partial\sigma/\partial\mathbf{k}$ is the vector group velocity in the moving frame. Subsequently, we will restrict our attention to the one-dimensional case $\mathbf{U} = (U, 0)$, $\mathbf{k} = (k, 0)$ where all propagation is in the $\pm x$ direction. (A recent discussion of the more general case of two-dimensional propagation in the present context is given by *Shyu and Tung* [1999].) For a wave propagating in the $+x$ direction we then have

$$C_{ga} = U + C_g. \quad (3)$$

Blocking occurs at points where the absolute group velocity C_{ga} falls to zero, which also corresponds to a singularity in the ray approximation for wave action transport where action density and wave height go to infinity. Setting C_{ga} to zero gives

$$C_g = -U. \quad (4)$$

The results of this study will show that the location of blocking predicted by the dispersion relation (1) can be strongly affected by nonlinear amplitude dispersion. The modification to theory needed to account for this effect is discussed in section 3.1.

[4] The dynamics of strong wave-current interactions have been studied for quite some time now. *Bretherton and Garrett* [1969] have shown that in the presence of a current it is the wave action that is conserved and not the wave energy. However, this conservation principle is based on ray theory approximations and fails close to the blocking point, which is a caustic in the ray theory. *Smith* [1975] and *Peregrine* [1976] obtained a uniformly valid linearized solution for the wave amplitude through the blocking region. They showed that around the blocking region the amplitude envelope is given by an Airy function, and away from the blocking region the wave field consists of an



Figure 1. Wave blocking at Indian River inlet, Delaware, USA.

incident wave and a much shorter reflected wave. More recently, *Shyu and Phillips* [1990] and *Trulsen and Mei* [1993] have extended the results to include the effects of surface tension which, if the reflected waves are short enough, leads to the waves being re-reflected from a second blocking point downstream of the primary gravity wave blocking point.

[5] These theories are based on the linear wave assumption and require that the incident waves be very small. In inlets these conditions are rarely satisfied (as is evident from

Figure 2) and most waves break at or before the blocking point without being reflected. Even those waves which do not get blocked lose a considerable amount of energy due to waves breaking on the strong currents. In contrast to the case of depth-limited wave breaking, there is a scarcity of experimental data to study current-limited wave breaking. *Lai et al.* [1989] have studied the kinematics of the strong interaction between waves and opposing currents but do not give any results about the dynamics. Their experimental data have been used by *Ris and Holthuijsen* [1996] to study



Figure 2. Wave field close to the blocking point.

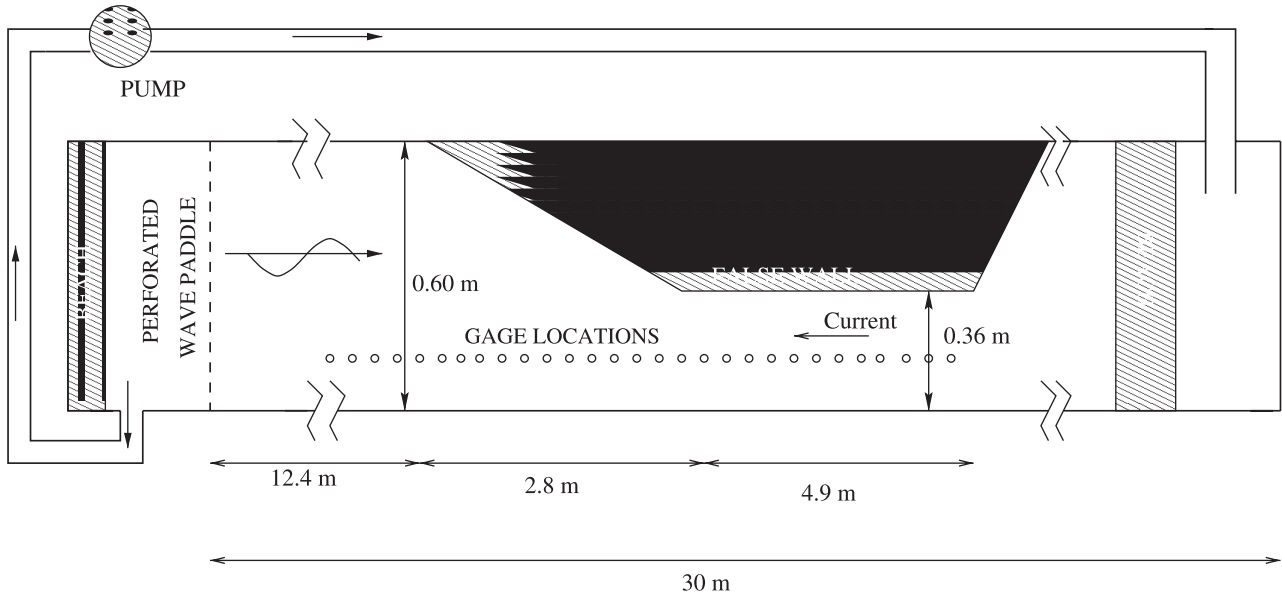


Figure 3. Schematic plan view of the experimental setup.

wave blocking in random waves, but the lack of data still leaves many questions unanswered.

[6] In this study a series of experiments have been conducted in order to develop a better understanding of the dynamics involved in the interactions between waves and strong opposing currents. Initial results from these experiments have been presented by *Chawla and Kirby* [1998], and a detailed description of the experiments is available from *Chawla and Kirby* [1999]. In this paper, we concentrate on the study of energy dissipation due to wave breaking at or before the blocking point. Both monochromatic and random wave tests are presented. Empirical dissipation formulae are proposed based on experimental results.

2. Experimental Setup

[7] The experiments were conducted in a 30 m long recirculating flume, shown schematically in Figure 3. Currents are generated using a 30 HP Weinmann pump that pumps water at a rate of $9463.5 \times 10^{-5} \text{ m}^3/\text{s}$ under a head of 60 feet. The pump draws water from behind the wave paddle and discharges into the flume at the other end. A flow straightener has been placed in the flume to remove large-scale eddies. A perforated “piston-type” wave paddle is used to generate waves in the tank. This allows us to draw out the water from behind the wave maker, and the vertical profile of the current in front of the wave paddle remains unchanged. The width of the flume is 0.6 m. All the experiments are conducted in a water depth of 0.5 m.

[8] An inlet was constructed by narrowing the width over a section of the flume with the help of a false wall. The width of the narrow channel is 0.36 m. The channel expands slowly (angle of $\sim 5^\circ$) to the width of the flume to prevent flow separation in the expansion. Thus the additional complexity of wave focusing on a laterally spreading jet is avoided. The experiments have been designed such that wave blocking occurs close to the narrow part of the inlet.

In tests both with and without currents, no significant three dimensionality of wave crests was observed except near periods of time $T = 1 \text{ s}$, for monochromatic tests in the presence of currents, which corresponds to the natural period of the first cross tank sloshing mode. This range of periods was subsequently excluded from the tests.

[9] The origin is placed at the beginning of the narrow part of the inlet with the x coordinate axis pointing down the length of the flume and positive in the direction of the waves. Thus the inlet begins at $x = -2.8 \text{ m}$, and the narrow part of the inlet extends from $x = 0$ to 4.9 m . Owing to symmetry, the side wall of the flume becomes the center line of the inlet. The y coordinate axis points positive toward the false wall with $y = 0$ at the centerline (right wall of the tank). The z coordinate axis points positive upward with $z = 0$ at the still water level.

[10] All current measurements have been made with the help of a SonTek acoustic Doppler velocimeter (ADV), while all of the wave measurements are made with the help of capacitance wave gauges. A detailed measurement of the vertical current profile both across and along the channel was carried out. Figure 4 shows the mean current (averaged over 300 s) profile at five different locations along the channel. The mean current has a slight shear due to the bottom boundary layer. There is also some slight variation across the width of the channel, consistent with the presence of sidewall boundary layers (see *Chawla and Kirby* [1999] for details). For the purposes of this study the variations over depth and width are ignored. The current is assumed to be uniform and given by

$$U \equiv -\frac{Q}{bh}, \quad (5)$$

where b is the width of the channel, h is the water depth, and Q is the volume flux. Q was measured with the help of a digital flow meter attached to the supply pipe. Boundary layer effects have been ignored in equation (5),

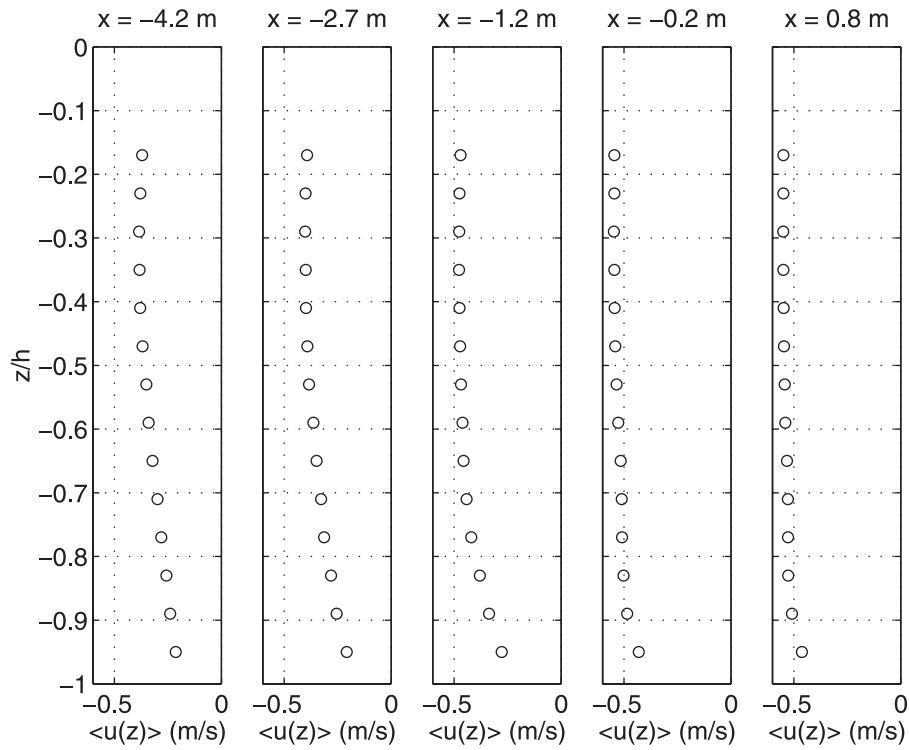


Figure 4. Vertical mean current profiles at five different locations in the channel.

leading to lower predicted mean currents. To account for this, the value of Q was artificially increased from 0.089 to $0.095 \text{ m}^3 \text{ s}^{-1}$ (see Figure 5).

[11] The wave periods for the different test cases range from 1.2 to 1.6 s. The corresponding kh values outside the narrow channel range from 1.35 to 2.4, where the Dop-

pler-shifted linear dispersion relation has been used to estimate the wavenumber. Within the narrow channel where the currents are stronger the waves are shorter, leading to higher values for kh . Thus the waves generated in the experiments can be classified as being intermediate-depth water waves. The narrowing channel causes the

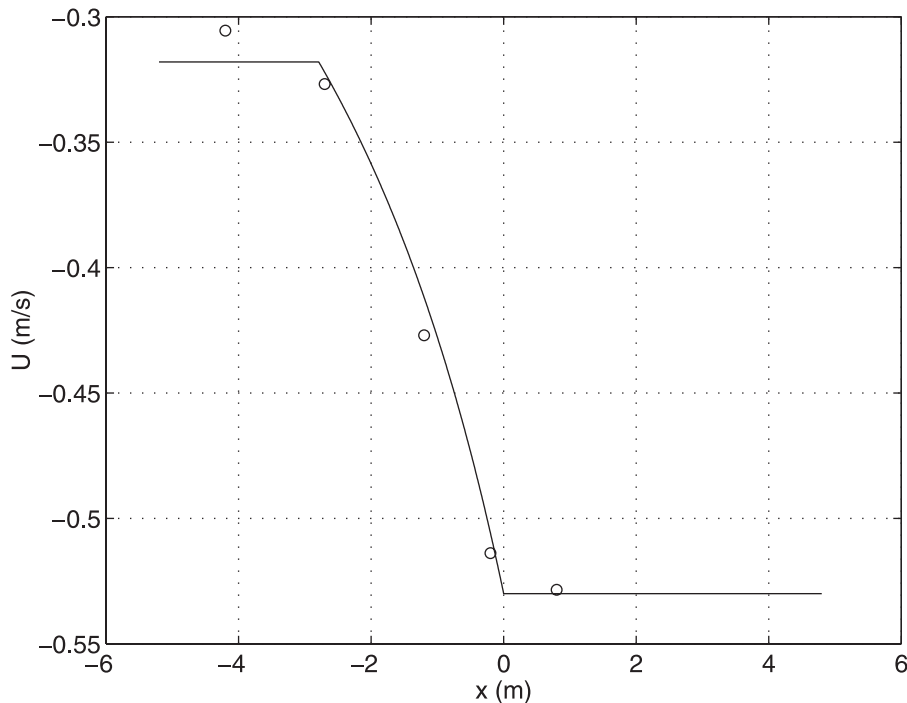


Figure 5. Average current as a function of x . Solid line shows Q/bh , and circles show data.

Table 1. Initial Conditions for Baseline Experiments Determined at $x = -5.3$ m

Test Condition	Period T_s , s	Wave Height H_s , m
Waves only	1.06	0.038
Waves and currents	1.08	0.048

waves to shoal even in the absence of an opposing current. To show the effects of an opposing current on the shoaling process, random wave experiments were conducted both in the presence and absence of currents. The initial conditions were measured at the first gauge (located outside the channel at $x = -5.3$ m) and are given in Table 1. Figure 6 shows the significant wave height H_s (normalized by the initial wave height), and the wave steepness $kH_s/2$, as a function of distance for the two different test conditions. The wave steepness is determined by using the linear Doppler-shifted dispersion relation and the peak wave period to estimate the wave number k . In the presence of an opposing current this parameter could only be computed up to $x = -1.3$ m, as the opposing current exceeded the linear blocking limit beyond this point. Also plotted in the figure is the transformation based on bulk conservation of wave action in the absence of a current. The figure shows that in the absence of a current, much of the wave shoaling is explained by the narrowing channel width. Some energy dissipation due to breaking of the largest waves is also observed in the narrow channel ($x > 0$). Though both the wave height and wave steepness increase more rapidly in

the presence of an opposing current, the increase in the wave steepness is enhanced because of the subsequent decrease in wavelength due to the increasing opposing current. This sharp increase in wave steepness leads to steepness limited wave breaking occurring earlier. In the narrow channel ($x > 0$), wave energy decreases much faster for the opposing current cases due to the combined action of wave blocking and wave breaking.

3. Monochromatic Wave Tests

[12] A total of 18 monochromatic wave tests were conducted, and the tests varied from very small wave heights in which the waves are reflected without breaking to cases with large wave amplitudes, where dissipation due to wave breaking is the dominant process. In this study we shall show results from 12 tests where wave breaking was observed. Each test consisted of 29 wave gauge measurements, with the starting gauge placed at $x = -5.2$ m. The test parameters are given in Table 2. Data were collected for 600 wave periods. Wave blocking conditions were satisfied for the 1.2-s waves and for some of the 1.3-s waves, while the 1.4-s waves were never blocked. Repeatability tests showed that the experiments were repeatable to within 6% error in wave height (see *Chawla and Kirby [1999]* for additional details). All statistical information about wave properties are extracted from the time series of the water surface with the help of a zero-upcrossing method. The zero-upcrossing method is a standard method used to divide a time series record into individual wave components. This

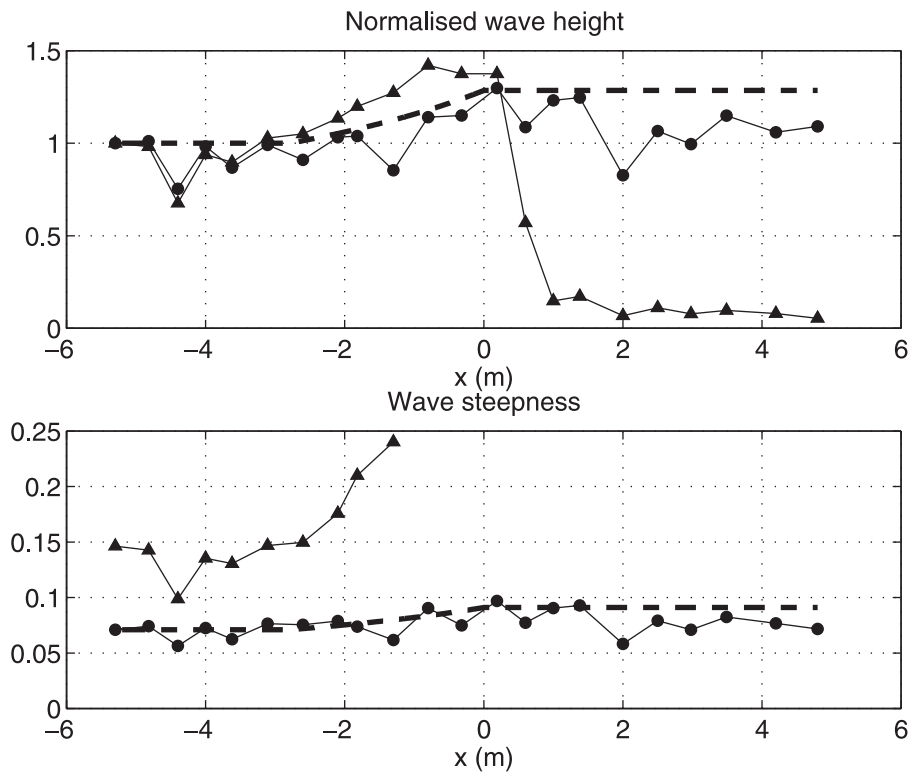


Figure 6. Normalized H_s and wave steepness ($kH_s/2$) as a function of x . Solid circles show waves without any currents; solid triangles show waves in the presence of an opposing current; and dashed line shows transformation due to conservation of wave action.

Table 2. Parameters for Monochromatic Wave Tests Determined at $x = -5.2$ m

Test	T , s	H , m	$kH/2$	kh
3	1.2	0.033	0.077	2.35
4	1.2	0.066	0.164	2.35
5	1.2	0.095	0.223	2.35
6	1.2	0.126	0.296	2.35
9	1.3	0.057	0.112	1.96
10	1.3	0.084	0.164	1.96
11	1.3	0.104	0.203	1.96
12	1.3	0.130	0.254	1.96
15	1.4	0.071	0.12	1.69
16	1.4	0.096	0.162	1.69
17	1.4	0.117	0.197	1.69
18	1.4	0.141	0.238	1.69

is performed by first subtracting the time-averaged signal from the record and then by denoting the individual waves by the points where the signal crosses the zero axis from below, hence the name zero-upcrossing method. Wave properties such as wave period and wave height are then determined for each wave component, from which statistical estimates such as the significant wave height are obtained.

3.1. Numerical Model for Monochromatic Waves

[13] A simple numerical model has been developed to study wave breaking. The model uses the wave action conservation principle first derived by *Bretherton and Garrett* [1969], given by

$$\frac{\partial}{\partial t} \left(\frac{E}{\sigma} \right) + \nabla \cdot \left(\frac{E}{\sigma} C_{ga} \frac{\mathbf{k}}{|\mathbf{k}|} \right) = 0, \quad (6)$$

where E is the wave energy density per unit surface area, C_{ga} is the group velocity, σ is the intrinsic wave frequency, \mathbf{k} is the wave number vector, and ∇ is the horizontal differential operator.

[14] Assuming steady wave conditions eliminates the first term in equation (6). Also, since we are trying to model wave flow in a narrow channel, flow variation across the channel is assumed to be small, and equation (6) is integrated over the width of the channel. Adding a dissipation term for wave breaking, the final model equation can be written as

$$\frac{1}{b} \left[\frac{\partial}{\partial x} \left(\frac{bEC_{ga}}{\sigma} \right) \right] = \frac{D}{\sigma}, \quad (7)$$

where b is the channel width and D determines the energy loss due to wave breaking. D is formulated below based on a bore dissipation analogy.

[15] *LeMéhauté* [1962] first hypothesized that the energy dissipation in a breaking wave can be modeled by the energy dissipation in a moving bore. This idea has been used with reasonable success in simulating depth-limited wave breaking [*Battjes and Janssen*, 1978]. Though the bore model has been derived for shallow water wave breaking, the same idea will be used here to determine an energy dissipation term for current-limited wave breaking.

[16] Consider a bore connecting two regions of uniform flow, illustrated in Figure 7. Using the control volume

approach, the energy dissipation per unit width across the bore is given by

$$D' = -\frac{1}{4} \rho g (h_2 - h_1)^3 \sqrt{\frac{g(h_2 + h_1)}{2h_2h_1}}. \quad (8)$$

[17] The length scales h_2 and h_1 can then be associated with the wave parameters

$$h_2 - h_1 \sim H \quad (9a)$$

$$\frac{(h_2 + h_1)}{2h_2h_1} \sim \frac{1}{\zeta}, \quad (9b)$$

where H is the wave height and ζ is a vertical length scale which needs to be prescribed. For depth-limited breaking models, ζ is given by the water depth h . However, for current-limited breaking models this would not be a useful scale, as wave breaking can occur in deep water as well. Instead, we use

$$\zeta = \frac{\tanh kh}{k}. \quad (10)$$

The advantage of using equation (10) is that the same vertical length scale is valid for shallow water ($\zeta \rightarrow h$) and deep water ($\zeta \rightarrow k^{-1}$). Substituting in the bore dissipation formulation gives

$$D' = -\frac{\beta}{4} \rho g H^3 \sqrt{\frac{gk}{\tanh kh}}, \quad (11)$$

where β is a nondimensional parameter which relates D' to energy dissipation in breaking waves. Now D' is the energy dissipation rate over the entire wave, and thus the dissipation rate per unit area is given by

$$D = \frac{D'}{L} = -\frac{\beta}{8\pi} \rho g k H^3 \left(\sqrt{\frac{gk}{\tanh kh}} \right). \quad (12)$$

In shallow water, equation (12) reduces to the standard bore model used in depth-limited wave breaking [*Battjes and Janssen*, 1978].

[18] Apart from an expression for energy dissipation we also need a criterion for the onset of wave breaking. Since wave breaking on opposing currents occurs due to the waves becoming very steep, a steepness limited criterion based on Miche's criterion is used:

$$\frac{kH_b}{\gamma \tanh kh} = 1, \quad (13)$$

where γ is a nondimensional parameter.

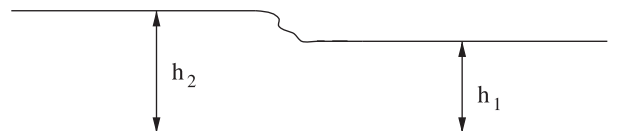


Figure 7. Sketch of a single steady bore.

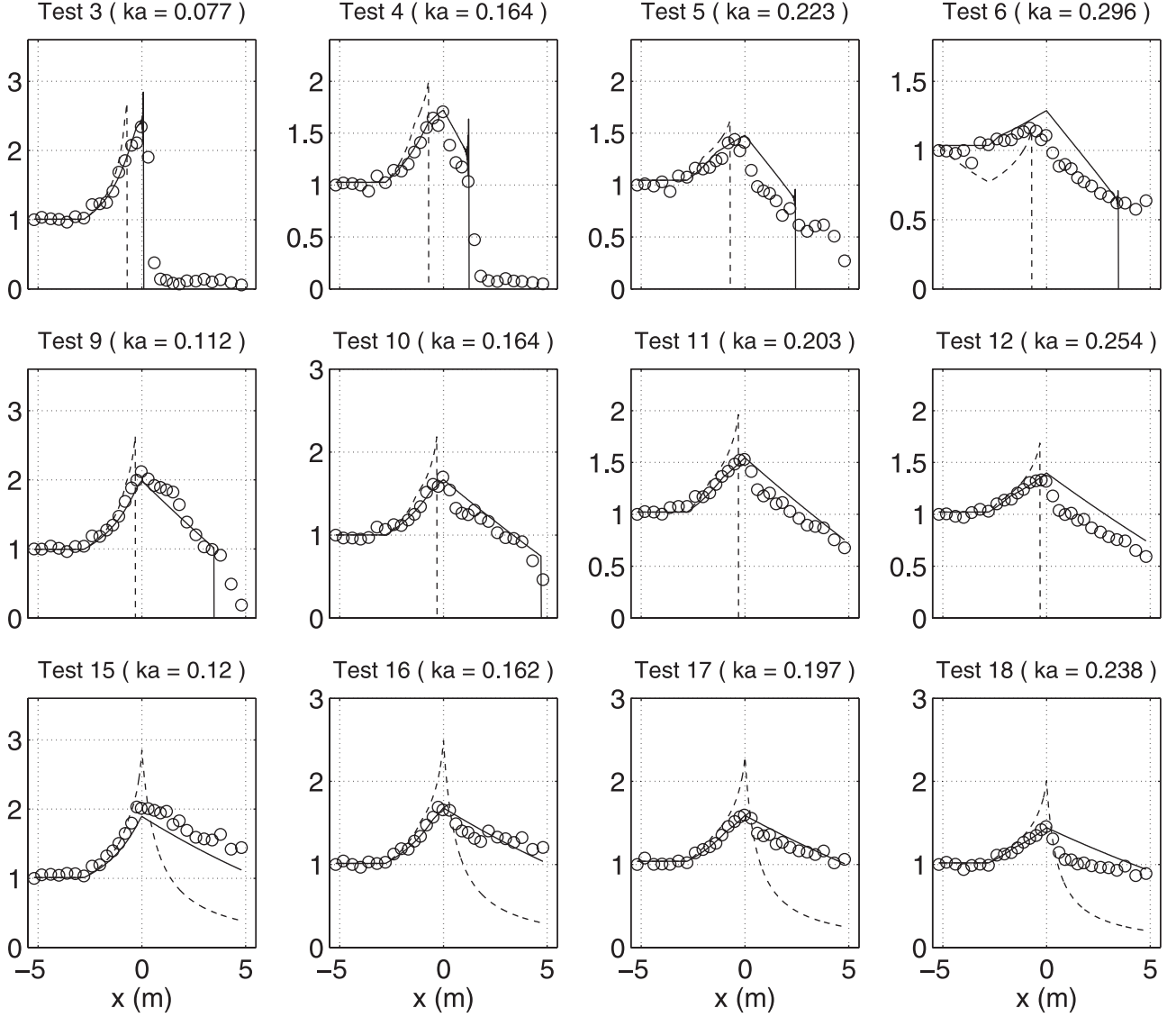


Figure 8. Normalized H for monochromatic wave tests. Solid line shows Stokes dispersion relation; dashed line shows linear dispersion relation; and circles show data. Initial wave steepness ka for the different tests are given in brackets. Initial wave periods, T_{pi} are as follows: tests 3–6, $T_{pi} = 1.2$ s; tests 9–12, $T_{pi} = 1.3$ s; tests 15–18, $T_{pi} = 1.4$ s.

[19] Equation (7) together with equations (12) and (13) provide a simple model for monochromatic waves shoaling and breaking on opposing currents. The model uses the wave action conservation principle and accounts for focusing due to a narrowing channel. Beyond the blocking point the roots of the dispersion relation become complex, as a result of which numerical simulations were stopped at the blocking point. Since the location of the blocking point is determined by the dispersion relation, the model is run using both a linear dispersion relation

$$\sigma = \sqrt{gk \tanh kh} \quad (14)$$

and a third-order Stokes dispersion relation

$$\sigma = \sqrt{gk \tanh kh \left[1 + (ka)^2 \left(\frac{8 + \cosh 4kh - 2 \tanh^2 kh}{8 \sinh^4 kh} \right) \right]} \quad (15)$$

to quantify the importance of amplitude dispersion in determining the model response.

3.2. Data to Model Comparison

[20] The parameters β and γ were fixed at 0.1 and 0.6, respectively, so that the energy dissipation in the model compares reasonably with data. In comparison, depth-limited breaking models usually set $\beta \approx 1$ and $\gamma \approx 0.7$ –0.8. The wave height comparisons are shown in Figure 8. The model works much better when using a Stokes dispersion relation. This is because close to the blocking point the waves steepen quite considerably, and terms of $O(ka)^2$ are no longer small enough to be neglected. The shoaling properties are quite accurately predicted by the wave action conservation principle if nonlinear dispersion is taken into account. We also find that a bore dissipation model does a reasonable job in predicting energy dissipation due to wave

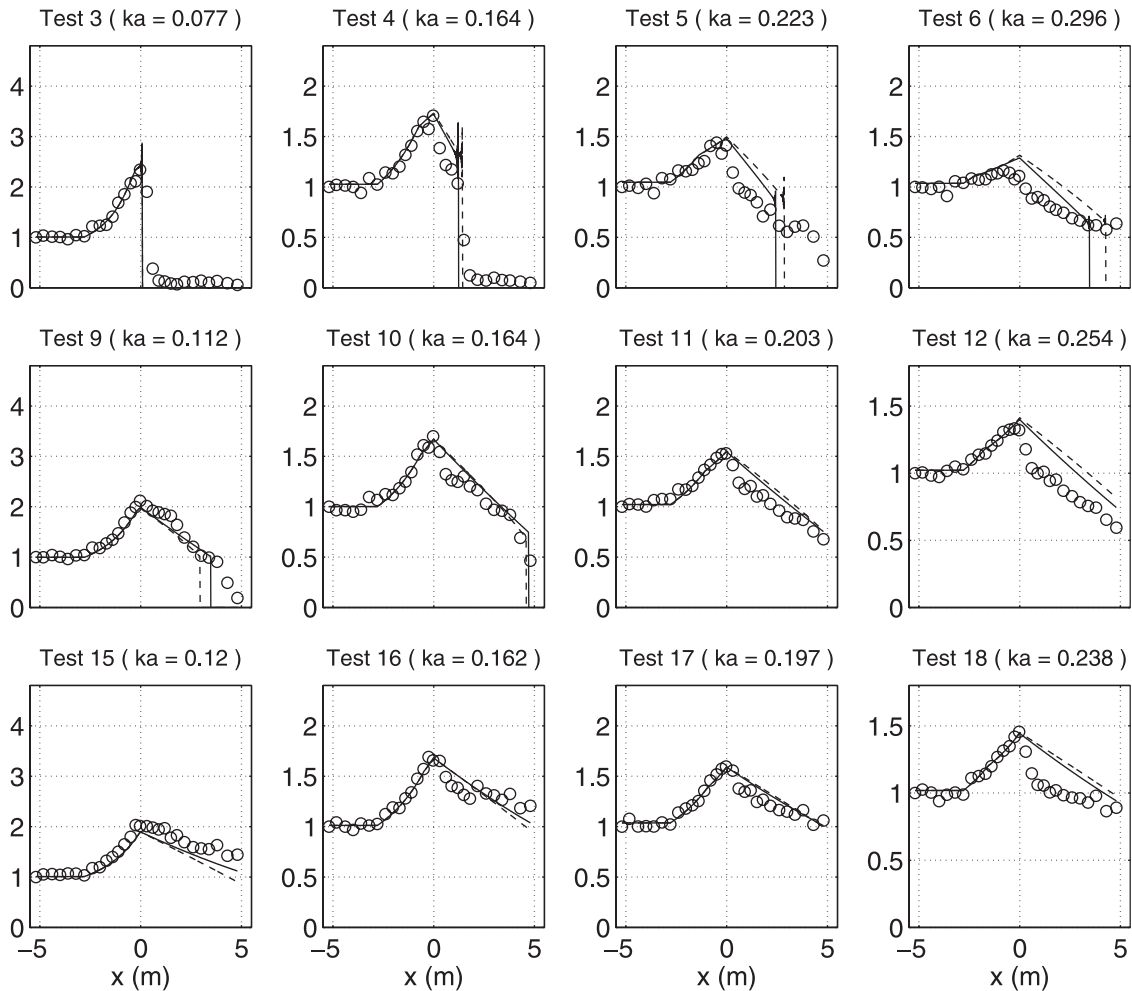


Figure 9. Normalized H for monochromatic wave tests. Solid line shows Bore model; dashed line shows whitecapping model; and circles show data. Initial wave steepness ka for the different tests are given in brackets. Initial wave periods, T_{pi} , are as follows: tests 3–6, $T_{pi} = 1.2$ s; tests 9–12, $T_{pi} = 1.3$ s; test 15–18, $T_{pi} = 1.4$ s.

breaking. In the case of test 6 the model results show a greater deviation between linear and nonlinear dispersion cases. This is because the waves are fairly steep, and since the linear dispersion relation predicts a larger wave steepness than the nonlinear dispersion relation, wave breaking occurs almost immediately in the simulation.

[21] Wave breaking in deep water is often described using a dissipation formula given by *Hasselmann* [1974]:

$$D = -\beta_c \sigma E, \quad (16)$$

where β_c is set to a value of 0.02 to provide a best fit to the present data. The comparison between the bore model and the whitecapping model is shown in Figure 9. The two models give similar results over the short distances used to calibrate model coefficients, and thus the tests are unable to distinguish between the qualitative behavior of the models.

[22] Another point that comes to attention is that although the blocking point is well predicted by the Stokes

dispersion relation, in cases like tests 3 and 4 the model fails in this respect in tests 5 and 6. To get an idea of why this happens, we take a look at the wave period distribution for all the tests (see Figure 10). The scatter in the wave period data in regions where the wave height goes to zero (tests 3, 4, and 9) is due to the noise in the signal and to the tendency of the zero-upcrossing method to perceive this noise as a propagating wave. This is a limitation of the zero-upcrossing method and is fortunately not a very strong limitation as the noise gets buried in the presence of a propagating wave.

[23] From Figure 10 we see that in tests 5 and 6 the waves shift continuously from a 1.2-s period to a 1.4-s period, for which the blocking conditions are not satisfied. This tendency is most pronounced in tests 5 and 6 but can also be seen to a smaller extent in tests 9 to 12. It is absent in the 1.4-s wave tests. The shift to longer wave periods occurs due to the development of sideband instabilities. *Benjamin and Feir* [1967] showed that water waves are unstable to sideband growth and that the growth of these instabilities depends upon the frequency and wave

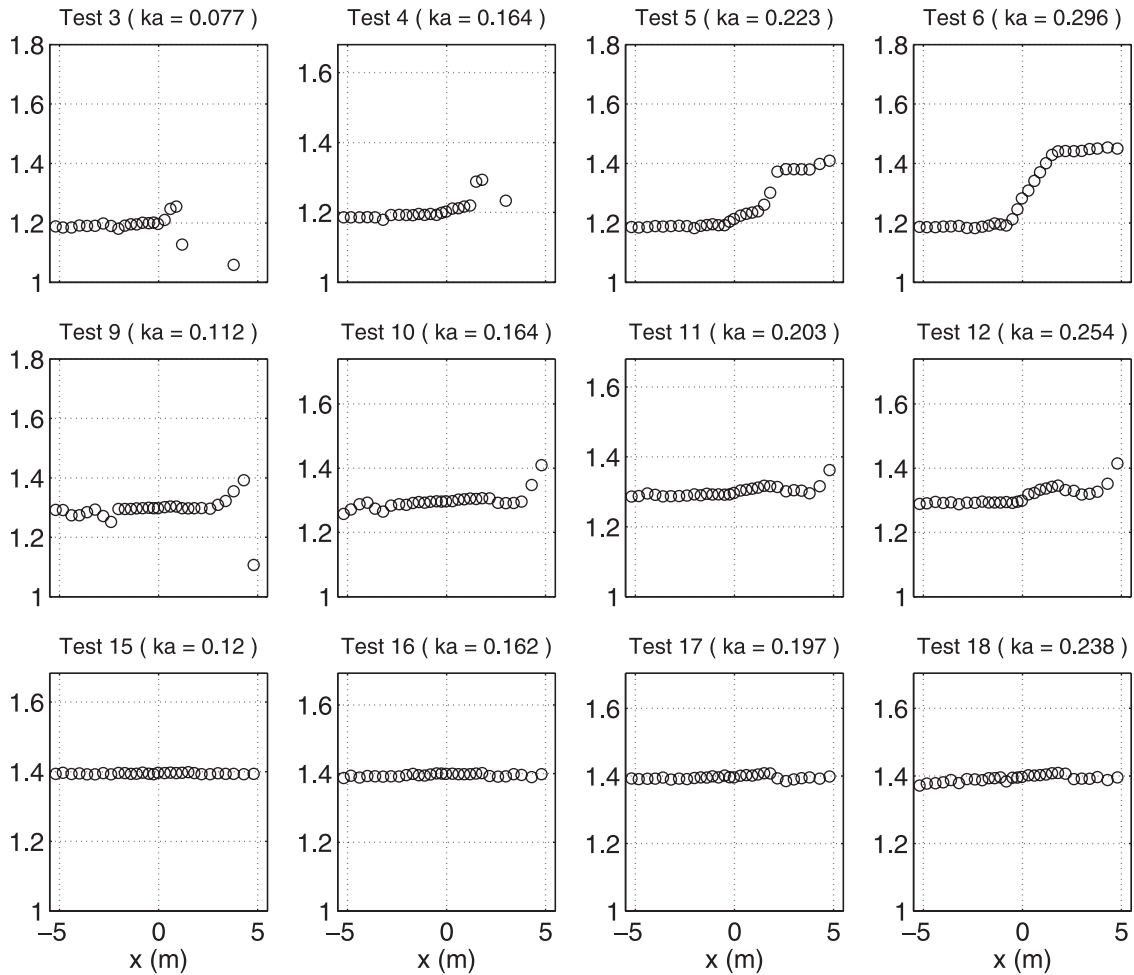


Figure 10. Measured wave period T_p for monochromatic wave tests. (Note the shift in wave energy to longer wave periods for the steeper waves in tests 5 and 6.)

amplitude. Due to the increase in wave steepness they become highly pronounced when the waves are riding on opposing currents and have been observed in the laboratory [Lai *et al.*, 1989]. Their effects become even greater as the waves approach the blocking point because the group velocity C_{ga} tends to zero, and the wave energy travels very slowly. Thus a significant amount of energy could be transferred from the primary wave to the sidebands even through small spatial distances, as the time available for the interaction to take place is large. *Trulsen and Dysthe* [1990] have shown that frequency downshifting can occur due to the selective damping of the upper sideband due to wave breaking. Here in the presence of a strong opposing current both the upper sideband and primary wave are blocked (according to linear wave theory) for the cases in question. The lower sideband requires a stronger blocking current than the primary wave or the upper sideband and continues to propagate forward. The mechanism thus appears to be distinct from that of *Trulsen and Dysthe* [1990]. This effect can be clearly observed in the frequency spectra for test 6 (see Figure 11). As the current increases, the energy is transferred to the lower sideband, while the upper sideband and primary wave component become blocked. In particular, note that between

$x = -0.5$ m and $x = -0.03$ m the energy in the lower sideband increases by almost 10 times. The occurrence of this effect depends both upon the growth of the sideband instabilities and the position of the primary wave component in the frequency spectrum. Our simple model cannot simulate this phenomenon. An attempt has been made to develop a third-order wave amplitude model to try and simulate this phenomenon and shall be reported separately.

4. Random Wave Tests

[24] The random wave experiments consisted of 20 spectral tests, the details of which are available from *Chawla and Kirby* [1999]. For each spectral test, gauge measurements were made at 36 different locations in the flume. At each location the time series of the water surface was recorded at 50 Hz for 1000 s. The tests varied from most of the spectrum being blocked in the case of test 1 to mild wave breaking without any blocking in test 20. Wave breaking occurred in all of the spectral tests. Since there are qualitative similarities between the different test cases, results from six representative tests shall be shown in this section.

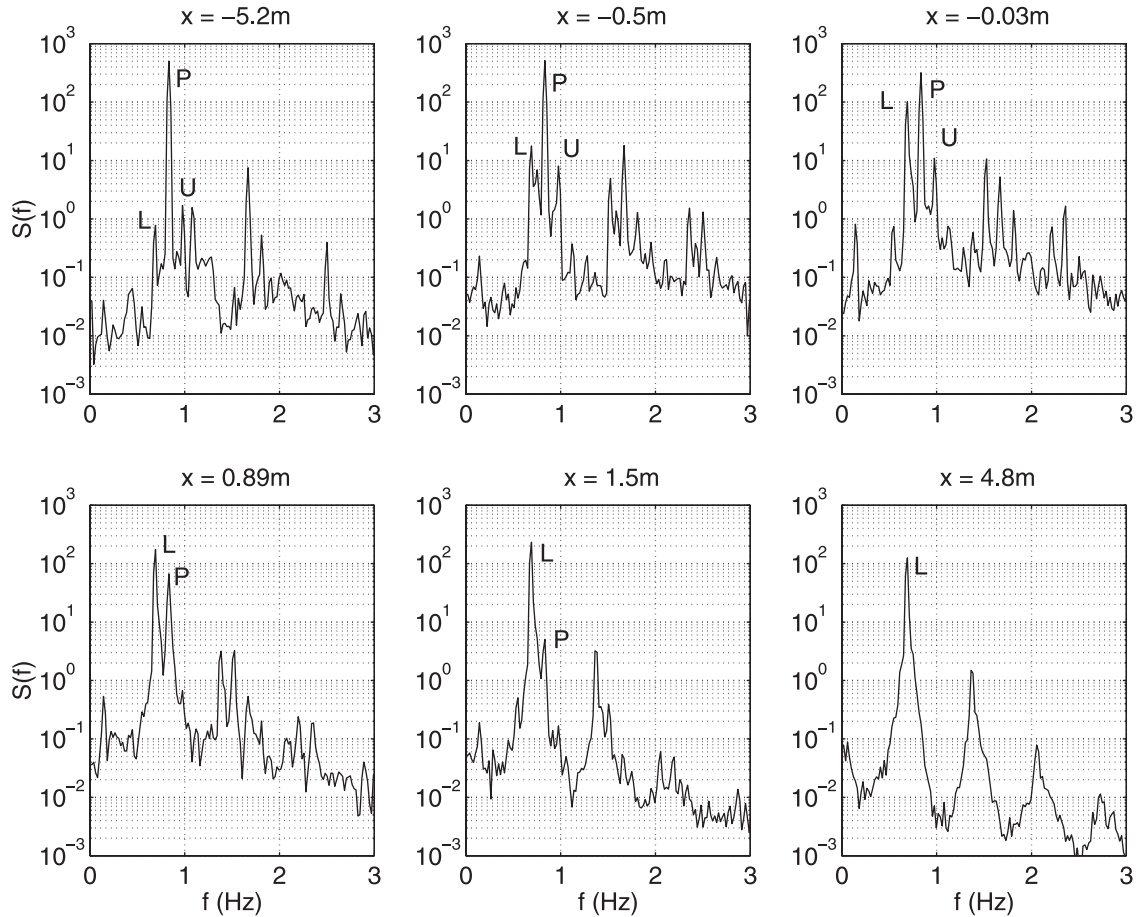


Figure 11. Frequency spectra for test 6 (initial $ka = 0.296$) at different locations (“L” shows the lower sideband, “P” shows the primary wave component, and “U” shows upper sideband). The value of x is the distance from the beginning of the narrow part of the channel.

[25] The experiments were designed such that for each test case the spectral shape of the signal sent to the wavemaker correspond to that of an equilibrium trimethyl aluminum (TMA) spectrum, which is a self-similar spectral shape used to describe wind waves in waters of finite depth [Bouws *et al.*, 1985]. However, due to wave blocking of high-frequency components, the measured spectra at the first gauge ($x = -4.6$ m) are narrow and do not correspond in shape to an equilibrium TMA spectrum at the higher frequencies (see Figure 12 for a typical spectrum). The initial conditions are therefore determined from the measurements of the first gauge. The spectra have been quantified in terms of the root-mean-square wave height H_{rms} and the average frequency $\bar{\omega}$.

$$\bar{\omega} \equiv 2\pi \frac{\int_0^\infty f S(f) df}{\int_0^\infty S(f) df} \quad (17)$$

The parameters for the full set of tests are given in Table 3. Larger values of H_{rms} were not used because they led to considerable wave breaking at the wavemaker paddle itself.

4.1. Bulk Dissipation Formula

[26] Before developing a numerical model for random waves we need to determine a bulk dissipation formula for

random waves breaking on opposing currents. Similar to the monochromatic wave problem, we shall use a previous method for determining bulk dissipation in depth-limited random wave breaking [Thornton and Guza, 1983] (hereinafter referred to as TG83) as a guideline to solve for a bulk dissipation formula for current-limited wave breaking.

[27] The basic assumption of TG83 is that the energy dissipation in any individual breaking wave is given by the bore model (see equation (12)). The bulk energy dissipation due to all the breaking waves is then given by

$$\langle D \rangle = \int_0^\infty D(H) P_b(H) dH, \quad (18)$$

where $P_b(H)$ is the probability distribution of wave height of the broken waves and D is the energy dissipation in the breaking wave. Using the bore model together with an empirical function for $P_b(H)$, TG83 determined the bulk dissipation to be

$$\langle D \rangle_{\text{tg}} = \frac{3\sqrt{\pi}}{16} \rho g \beta_r \bar{f} \frac{H_{\text{rms}}^5}{\gamma_r^2 h^3} \left[1 - \frac{1}{\left(1 + (H_{\text{rms}}/\gamma_r h)^2\right)^{5/2}} \right], \quad (19)$$

where β_r and γ_r are empirical parameters and h is the water depth. Equation (19) cannot be used to model deep water

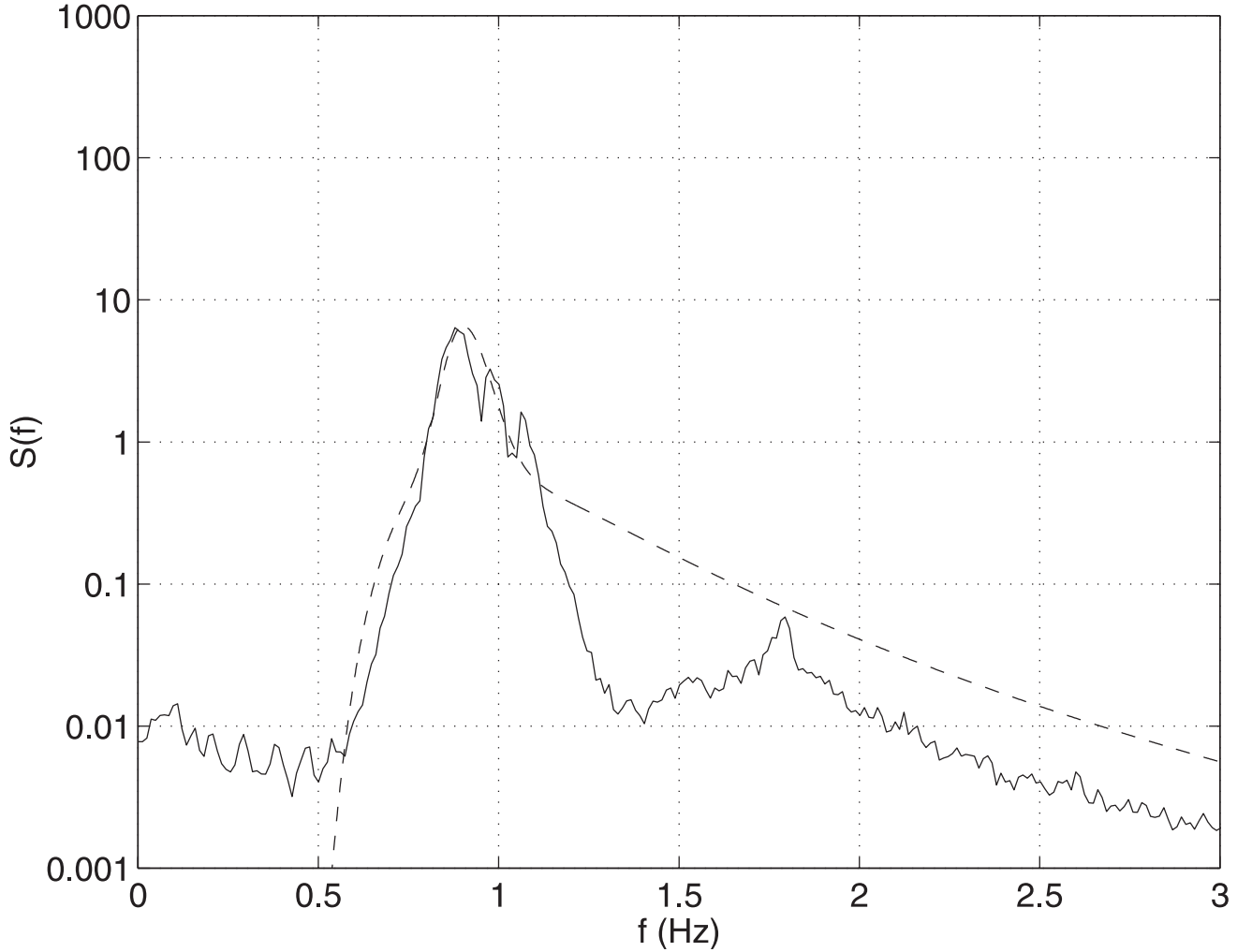


Figure 12. Energy spectra at the first gauge for test 1. Dashed line corresponds to a trimethyl aluminum (TMA) spectrum. The spectral shapes for remaining tests are similar; they differ in energy and peak frequency.

current-limited wave breaking in its present form due to its exclusive dependence on the water depth.

[28] To develop a modified form of the bulk dissipation formula, an empirical expression for $P_b(H)$ of broken waves in an opposing current needs to be obtained from experimental data. In order to do so, we must first be able to separate the breaking waves from the nonbreaking waves in any given time series.

4.1.1. Geometric Criterion for Breaking Waves

[29] A geometric criterion is used to separate out the breaking and nonbreaking waves in a time series. This criterion was first proposed by *Longuet-Higgins and Smith* [1983] and was later modified by *Xu et al.* [1986].

[30] The method consists of dividing the time series into individual wave components using the zero-upcrossing method. For each wave component we then determine

$$R = \left| \frac{\partial \eta}{\partial t} \right| \approx \left| \frac{\Delta \eta}{\Delta t} \right|. \quad (20)$$

Using the nondispersive wave equation

$$\frac{\partial \eta}{\partial t} + c \frac{\partial \eta}{\partial x} = 0, \quad (21)$$

we get

$$R \approx \left| c \frac{\Delta \eta}{\Delta x} \right|, \quad (22)$$

where c is the phase speed of the wave component determined using linear theory. Now

$$\frac{\Delta \eta}{\Delta x} \approx \tan \alpha,$$

where $\tan \alpha$ is the wave slope. *Longuet-Higgins and Fox* [1977] showed that $\tan \alpha = 0.586$ is the limiting slope for waves. Thus a wave is breaking if

$$R_{\max} \geq 0.586c, \quad (23)$$

Table 3. Parameters for Random Wave Tests Determined at $x = -4.6$ m

Test	$\bar{\omega}$, s^{-1}	H_{rms} , m	$\bar{k} H_{rms}/2$	$\bar{k} h$
1	5.81	0.026	0.081	3.098
2	5.68	0.033	0.096	2.897
3	5.40	0.042	0.106	2.53
4	5.33	0.045	0.110	2.45
5	5.35	0.026	0.064	2.474
6	5.24	0.034	0.08	2.35
7	5.07	0.047	0.102	2.174
8	5.03	0.057	0.122	2.135
9	5.07	0.033	0.072	2.174
10	4.96	0.046	0.095	2.068
11	4.85	0.059	0.116	1.97
12	4.80	0.068	0.131	1.928
13	4.90	0.033	0.067	2.015
14	4.76	0.044	0.083	1.894
15	4.70	0.058	0.107	1.846
16	4.63	0.070	0.125	1.791
17	4.60	0.027	0.048	1.768
18	4.45	0.040	0.066	1.658
19	4.39	0.052	0.084	1.617
20	4.28	0.062	0.096	1.544

where R_{max} is the maximum value of R (determined from equation (20) within each wave component. Equation (23) together with equation (20) provides a geometric criterion to determine breaking waves from a time series. The criterion is so called because it is based on the maximum slope of the waves. The biggest disadvantage with using this method is that some of the waves start breaking earlier and continue to break as they pass over the gauge, but by then their slope has reduced considerably. In addition, the method cannot distinguish between these breaking waves and unbroken waves with small slopes.

[31] To test the method, an experiment was conducted in which the time series of breaking random waves was recorded at eight different locations in the tank. Observers were placed in front of each gauge with a counter to record the broken waves passing over the gauges. The comparison between the probability of breaking (fraction of breaking waves) determined with the help of visual observations and the geometric method is shown in Figure 13.

[32] Though the qualitative distribution pattern of $Q_b(x)$ is reasonably reproduced, there are considerable discrepancies in the actual values. These discrepancies occur due to the errors in visual observations and the inability of the method to distinguish between broken and unbroken waves of small slope. However, since the dissipation formula is scaled by a nondimensional parameter, lack of quantitative agreement is not a big limitation. It is important to be able to determine the distribution of $Q_b(x)$, as this dictates how energy dissipation varies spatially. Thus the method shall be used to identify breaking waves.

4.1.2. Probabilistic Distribution Function for Breaking Waves

[33] An empirical formulation of the probabilistic wave height distribution of the broken waves is determined with the help of the experimental data. Figure 14 shows the distribution of broken and unbroken waves at $x = 0$ (where there is maximum wave breaking) for six representative tests. The solid line is the Rayleigh distribution. From the figure we see that the distribution of the broken waves is skewed toward the larger wave heights. This is qualitatively

similar to the results of TG83. Following their approach, the empirical probability density function (pdf) of broken waves shall be represented as a weighting function of the Rayleigh distribution

$$P_b(H) = W(H)P_r(H), \quad (24)$$

where $P_b(H)$ is the pdf of the broken waves, $W(H)$ is a weighting function to be determined, and $P_r(H)$ is the Rayleigh wave height distribution given by

$$P_r(H) = \frac{2H}{H_{rms}^2} \exp\left(-\left(\frac{H}{H_{rms}}\right)^2\right). \quad (25)$$

H_{rms} is the root-mean-square wave height.

[34] The weighting function $W(H)$ must be skewed toward larger values of wave height. Also, the proportion of waves breaking must increase with stronger opposing currents. Since waves tend to steepen on the stronger currents, a wave slope criterion is proposed for the weighting function

$$W(H) = \left[\frac{\bar{k}H_{rms}}{\gamma_r \tanh \bar{k}h}\right]^2 \left\{1 - \exp\left[-\left(\frac{\bar{k}H}{\gamma_r \tanh \bar{k}h}\right)^2\right]\right\} \quad (26)$$

where γ_r is a parameter to be determined and \bar{k} is the wave number corresponding to $\bar{\omega}$. The terms in the curly bracket skew the wave height distribution to larger wave heights.

[35] Substituting equations (26) and (25) in equation (24), we get an expression for $P_b(H)$ as

$$P_b(H) = 2H \left(\frac{\bar{k}}{\gamma_r \tanh \bar{k}h}\right)^2 \exp\left[-\left(\frac{H}{H_{rms}}\right)^2\right] \cdot \left\{1 - \exp\left[-\left(\frac{H}{H_{rms}}\right)^2 \left(\frac{\bar{k}H_{rms}}{\gamma_r \tanh \bar{k}h}\right)^2\right]\right\}. \quad (27)$$

[36] Figure 15 gives the comparison between the pdf of broken waves and the empirical function given in equation (27). There is no curve for test 1 because $x = 0$ is beyond the blocking point of the waves, and hence \bar{k} in equation (27) is not defined for test 1 at this point (see Figure 17). The probability of breaking Q_b can then be obtained from the pdf by

$$Q_b = \int_0^\infty P_b(H) dH. \quad (28)$$

The value of γ_r is fixed by comparing the probability of breaking obtained from equations (28) and (27) and the probability of wave breaking obtained from counting the breaking waves in the experimental data. Figure 16 shows comparisons for several representative cases as a function of x for $\gamma_r = 0.6$.

[37] Substituting equation (27) together with the bore energy dissipation formula in equation (18) gives

$$\langle D \rangle = \frac{-3\beta_r \rho}{32\sqrt{\pi}} \sqrt{\frac{(g\bar{k})^3}{\tanh \bar{k}h}} \cdot \left(\frac{\bar{k}}{\gamma_r \tanh \bar{k}h}\right)^2 H_{rms}^5 \left[1 - \left\{1 + \left(\frac{\bar{k}H_{rms}}{\gamma_r \tanh \bar{k}h}\right)^2\right\}^{-5/2}\right] \quad (29)$$

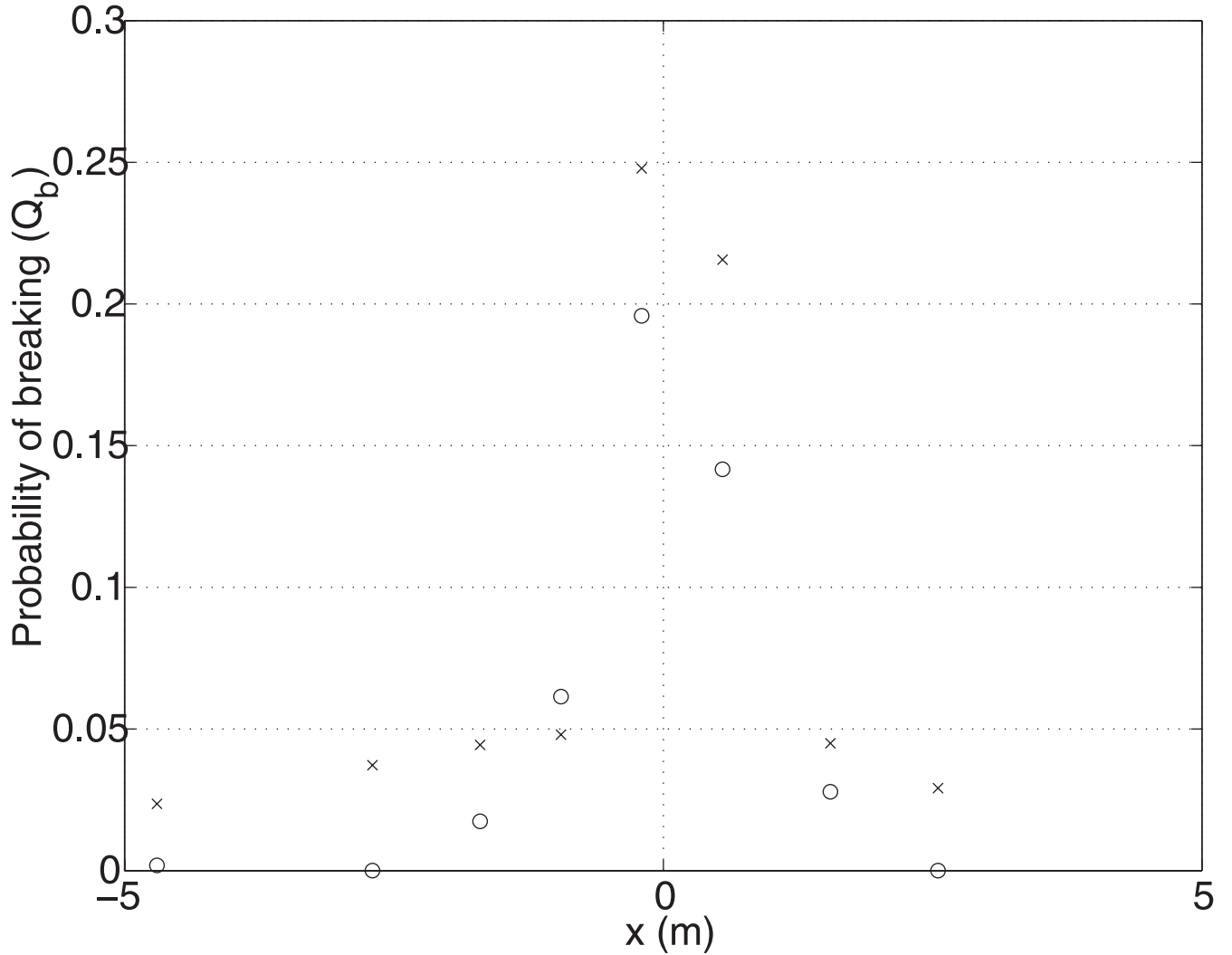


Figure 13. Probability of breaking Q_b as a function of x . Circles show geometric method; and crosses show measured probability by counter.

Equation (29) is an expression for bulk dissipation in random breaking waves, based on a wave steepness formulation, and can be used for simulating deep water steepness limited breaking. Furthermore, in shallow water, where $\tanh kh \rightarrow kh$, equation (29) reduces to the expression obtained by TG83. It should be mentioned that we could have chosen a different form for $P_b(H)$ to give a better comparison with the distribution of broken waves, but the subsequent expression for bulk energy dissipation would have been very complex. We would also lose the added advantage of equation (29), reducing to the depth-limited form of TG83 in shallow water.

4.2. Numerical Model

[38] Using the wave action conservation principle together with an expression for the bulk energy dissipation, two simple numerical models are used. Since we have already seen from the monochromatic tests that amplitude dispersion effects are important, a nonlinear dispersion relation is used in both the models. H_{rms} is used to quantify the amplitude dispersion effects.

4.2.1. Bulk Wave Action Conservation Model

[39] In this model the individual spectrum is described by its bulk quantities and is then modeled as a monochromatic wave using the bulk dissipation formula for wave breaking. The governing equation is given by

$$\frac{1}{b} \left[\frac{\partial}{\partial x} \left(\frac{bE_{rms}\bar{C}_{ga}}{\bar{\sigma}} \right) \right] = \frac{\langle D \rangle}{\bar{\sigma}}, \quad (30)$$

where $E_{rms} = \frac{1}{8}\rho g H_{rms}^2$ is the wave energy corresponding to H_{rms} . \bar{C}_{ga} and $\bar{\sigma}$ are the group velocity and intrinsic wave frequency associated with the average frequency $\bar{\omega}$.

[40] A significant problem with this model is that we specify an $\bar{\omega}$ in the initial conditions, which characterizes the spectrum. In the model this $\bar{\omega}$ remains fixed as the random waves progress into stronger currents. However, in reality, as the waves move into stronger currents, more of the higher frequency components become blocked, and subsequently $\bar{\omega}$ shifts down. We thus do not expect the

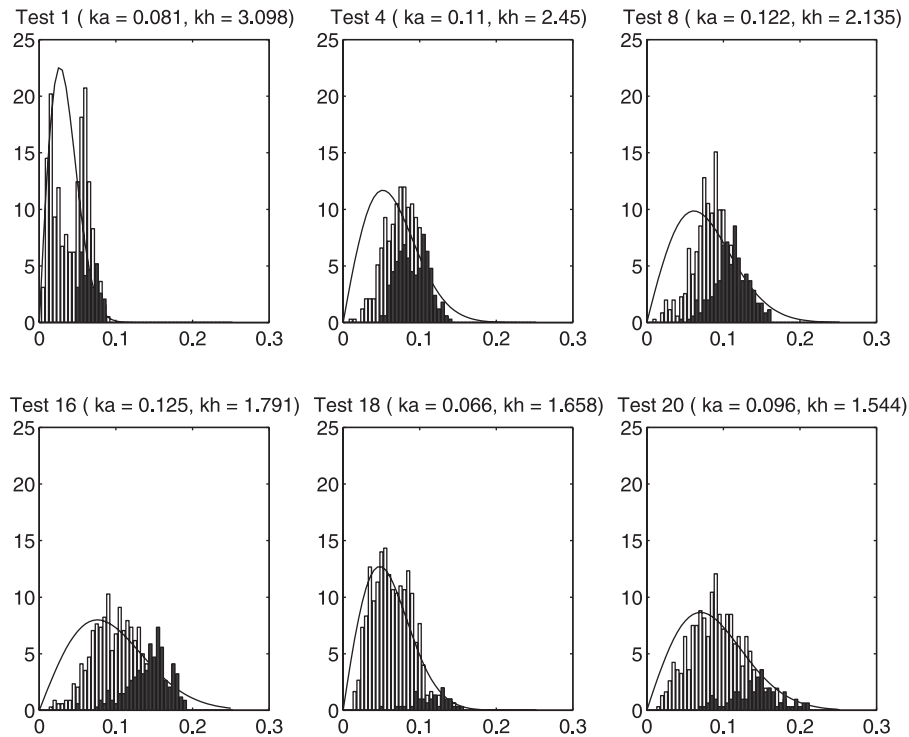


Figure 14. Probability distribution of broken (solid bars) and unbroken waves (open bars) for different tests at $x = 0$. The solid line shows the Rayleigh distribution.

model to perform very well, particularly in regions where a large part of the spectrum is blocked.

4.2.2. Spectral Model

[41] A second model is used to account for the limitations of the first model. In this approach the entire spectrum is modeled and not just its bulk quantities. The model involves dividing the frequency spectrum into N equally spaced bins and representing the energy in each bin by a monochromatic wave. The governing equation for the i th wave component is then given by

$$\frac{1}{b} \left[\frac{\partial}{\partial x} \left(\frac{bE_i(C_{ga})_i}{\sigma_i} \right) \right] = \frac{\delta_i}{\sigma_i}, \quad (31)$$

where δ_i represents the energy dissipation in each frequency component due to wave breaking.

[42] The advantage of having spectral information is that we can empirically adjust δ_i so that the higher frequency components have greater energy dissipation. The expression used for δ_i is given by

$$\delta_i = \alpha E_i \left(\frac{\sigma_i}{\bar{\sigma}} \right)^4, \quad (32)$$

where α is a coefficient. Since the total energy dissipation from all the wave components is given by $\langle D \rangle$, we get

$$\alpha = \frac{\langle D \rangle}{\sum_{i=1}^N E_i \left(\frac{\sigma_i}{\bar{\sigma}} \right)^4}. \quad (33)$$

[43] Equation (31) together with equations (32), (33), and (29) make up the spectral model. The advantage of this model as compared with the bulk conservation model is that individual frequency components can be tracked separately, and we can simulate spectral quantities like $\bar{\omega}$ more accurately. The disadvantage is that it is computationally more intensive.

4.3. Comparisons With Data

[44] The parameters β_r and γ_r in the two models were fixed at 0.4 and 0.6, respectively. In the spectral model, 100 energy bins were used. For the spectral comparisons the energy spectra from the gauge measurements was Bartlett averaged with 24° of freedom ($\Delta f = 0.012$). The H_{rms} comparisons are shown in Figures 17 and 18. The disadvantages of representing an entire spectrum by just one component is seen in test 8, where only a part of the spectrum is blocked. Both models fare poorly in the case of test 4. This is because the waves in test 4 are short and steep and are subject to sideband instability effects, similar to the ones seen in test 6 for the monochromatic wave tests. Overall, the bulk dissipation formula for random waves breaking on a current works reasonably well. There are a few discrepancies between data and spectral model predictions of $\bar{\omega}$ because the spectral model can only predict the downshift due to the shoaling of the longer waves and subsequent dissipation of the steeper waves and ignores all nonlinear effects.

[45] The evolution of the spectrum and the comparison with the spectral model for one of the tests (test 16) is shown in Figure 19. The spectral model simulates the spectrum reasonably well, except in the narrow channel where the high-frequency components are underpredicted. Figure 20

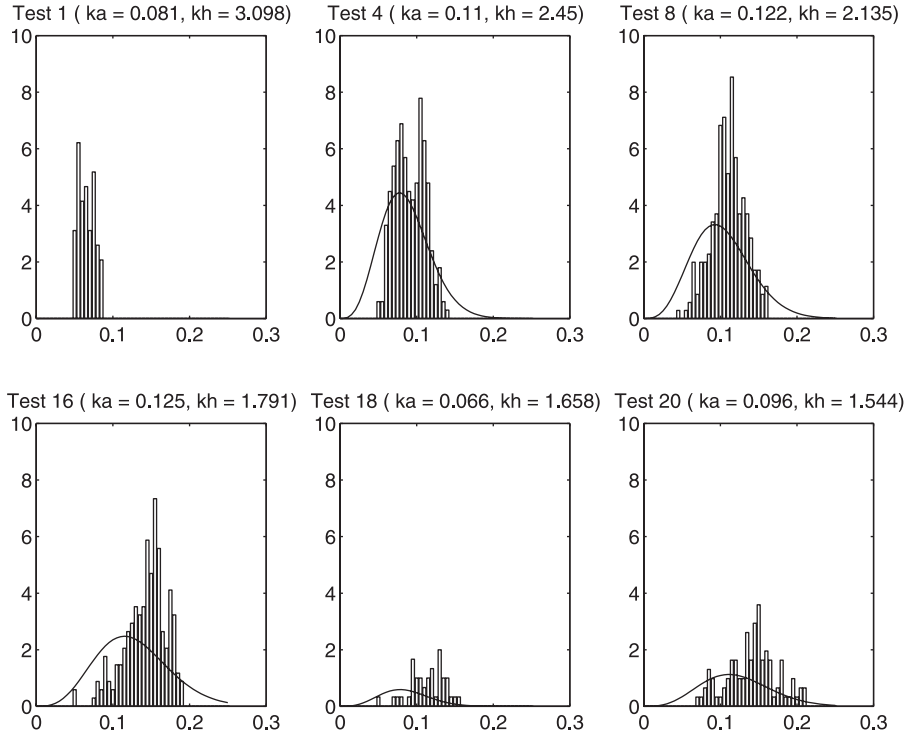


Figure 15. Probability distribution of broken waves (open bars) for different tests at $x = 0$. The solid line shows $P_b(H)$ given by equation (27).

shows the spectral comparisons between model results and data at the last gauge ($x = 4.6$ m) for representative tests. The spectrum of the first gauge has also been plotted to show the downshift more clearly.

[46] We thus find that a probability of breaking criterion based on the wave slope together with a bore dissipation model works reasonably well in simulating energy dissipation in random waves. Another criterion which was based

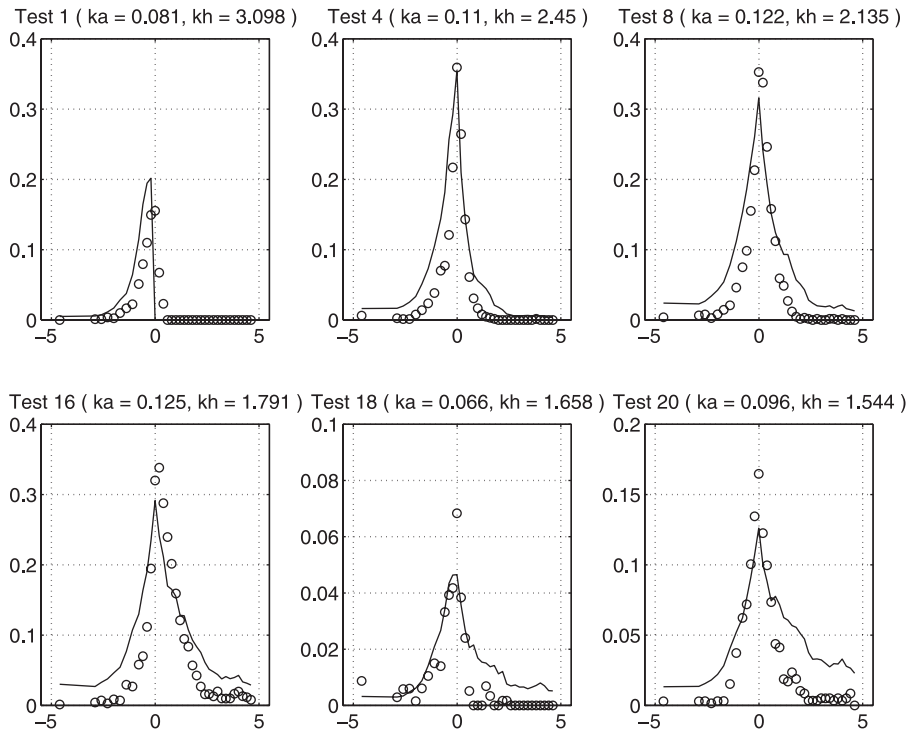


Figure 16. $Q_b(x)$ for representative tests. Circles show geometric method; and solid line shows empirical probability density function.

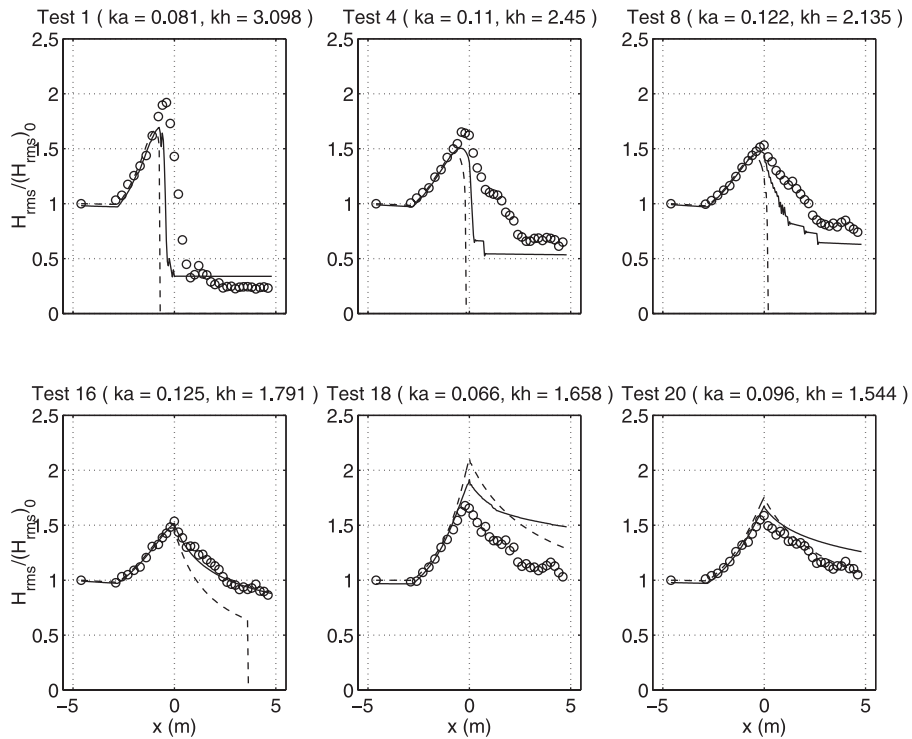


Figure 17. Normalized H_{rms} for representative tests. Solid line shows the spectral model; dashed line shows the bulk model; and circles show data. Initial wave steepness ka is given within brackets.

on wave slope was given by [Battjes and Janssen 1978]. Though their model was derived for depth-limited wave breaking, we should be able to use their model with a few

modifications to simulate current-limited wave breaking. They state that all of the waves breaking at any given point have a wave height H_{max} , which is the maximum wave

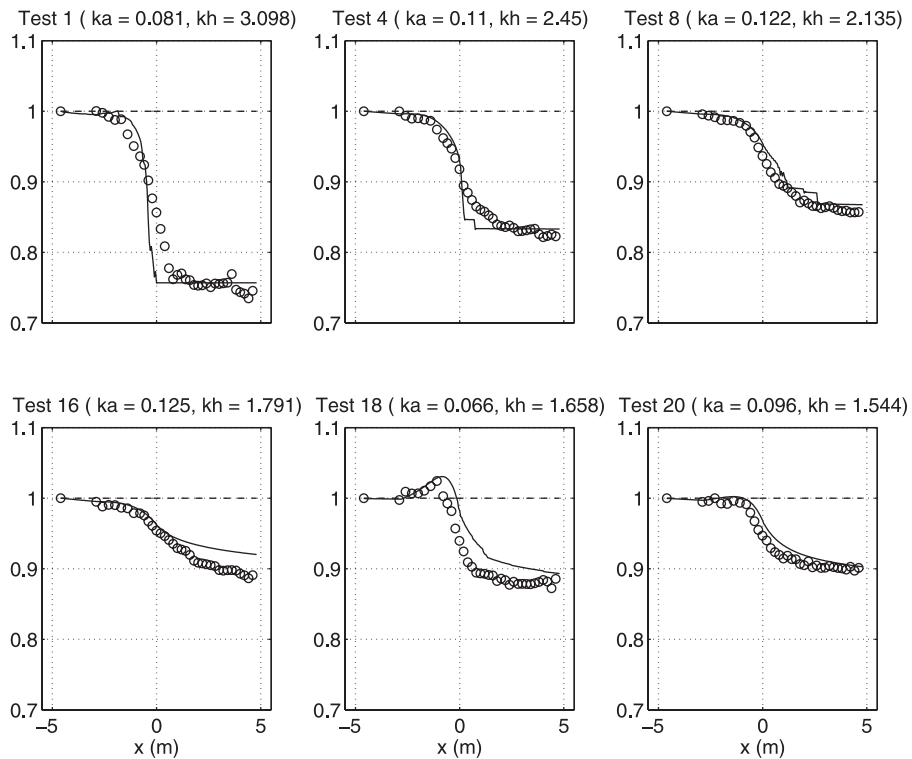


Figure 18. Normalized $\bar{\omega}$ for representative tests. Solid line shows the spectral model; dashed line shows the bulk model; and circles show data. Initial wave steepness ka is given within brackets.

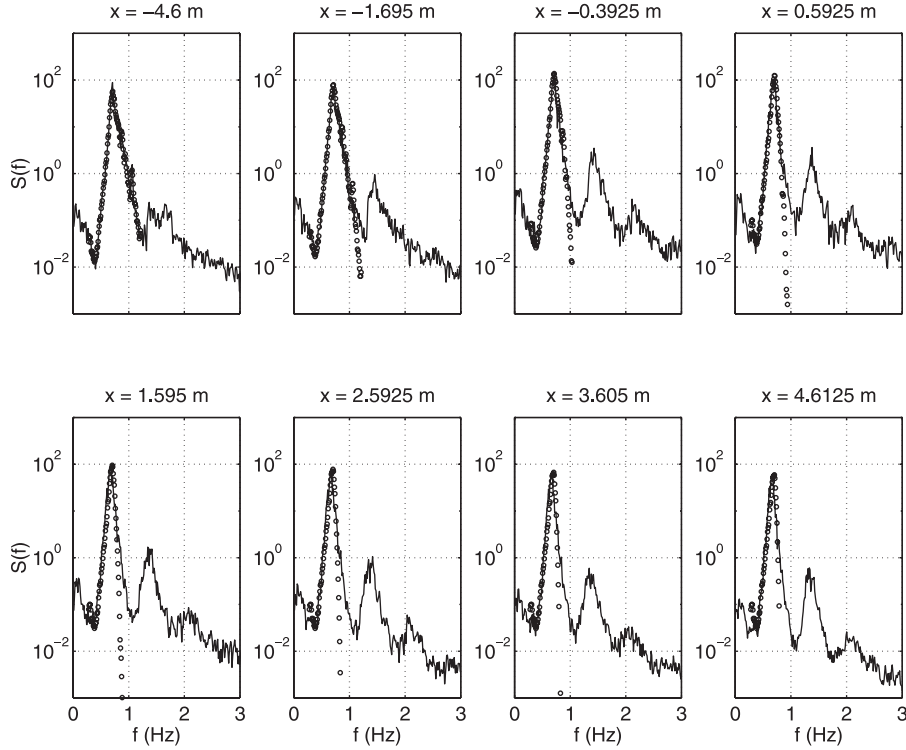


Figure 19. Energy spectra for test 16. Circles show the spectral model; and solid line shows data.

height. For the current-limited breaking cases we shall denote this by

$$H_{\max} = \frac{\gamma_r}{k} \tanh kh, \quad (34)$$

which is very similar to the breaking criterion used for monochromatic waves (see equation (13)). They then determined an expression for the probability of breaking (Q_b) in terms of a transcendental equation using a Rayleigh distribution.

$$\frac{1 - Q_b}{\ln Q_b} = - \left(\frac{H_{\text{rms}}}{H_{\max}} \right)^2 \quad (35)$$

Using the bore dissipation model, the energy dissipation is then given by

$$D_{bj} = -\beta_r Q_b \frac{\rho}{8\pi} \left(\sqrt{\frac{(g\bar{k})^3}{\tanh kh}} \right) H_{\max}^3. \quad (36)$$

[47] Using the same parametric values and the spectral model formulation, the comparison between the present bulk dissipation formula given by equation (29) and the Battjes and Janssen dissipation formula given by equation (36) are shown in Figure 21. Both formulae give very similar results.

5. Monochromatic Wave Breaking Versus Random Wave Breaking

[48] Energy dissipation due to current-limited wave breaking has been formulated using a modified bore dis-

sipation formula. Similar to the depth-limited breaking models [Thornton and Guza, 1983; Battjes and Janssen, 1978], the only difference between the monochromatic dissipation formulation and the random wave bulk dissipation formulation is the probability of breaking used in the random wave formulation, which is based on a prescribed wave height distribution of the breaking waves. However, unlike the depth-limited breaking models, the coefficient β that is used in the current-limited breaking models to quantify energy dissipation has different values for monochromatic and random waves (0.1 and 0.4, respectively).

[49] There are two possible causes for this disparity. The first is that in our tests the current does not increase monotonically and reaches a maximum in the narrow part of the channel. Thus the breaking process reduces as the waves propagate into the channel. This effect is accounted for in the random wave model because the probability of breaking reduces considerably (due to a reduction in wave steepness) in the narrow part of the channel, leading to a reduction in the energy dissipation. The monochromatic model, however, has been designed to continue dissipating energy once the breaking criterion is satisfied and does not account for waves not continuing to break. As a result, the breaking parameter β is calibrated to a lower value. The shallow water breaking models of Thornton and Guza [1983] and Battjes and Janssen [1978] have been calibrated on monotonic beaches. The second, and more likely, cause for the disparity is the sensitivity of the dissipation formulation to wave steepness. This is true more so for the random wave bulk dissipation formulation because wave steepness plays an important role in both the bore dissipation formulation and the probability of breaking (see equation (29)). In the random wave tests the wave steepness for

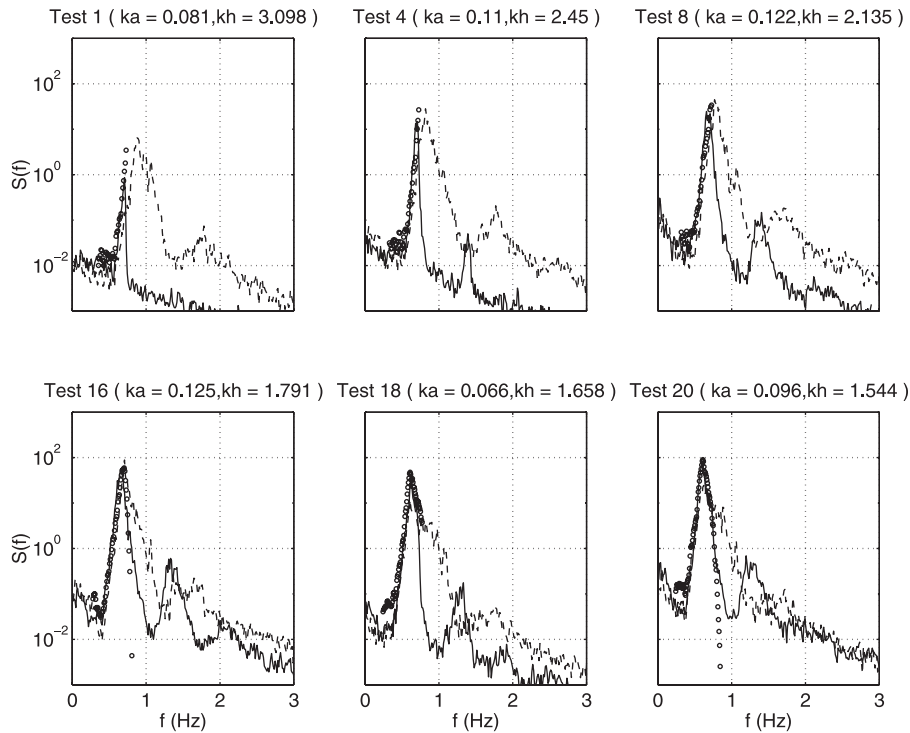


Figure 20. Energy spectra comparisons for representative tests. Dashed line shows data at $x = -4.6$ m; solid line shows data at $x = 4.6$ m; and circles show spectral model at $x = 4.6$ m.

the bulk energy dissipation is quantified by the average wavenumber \bar{k} . However, as the waves propagate against the increasing current, the average frequency $\bar{\omega}$ (which is used to compute \bar{k}) downshifts due to both nonlinear effects

and a combination of shoaling at the lower frequency components and blocking/breaking at the higher frequency components of the spectrum (see Figure 18). This downshift decreases \bar{k} and subsequently so does the energy dissipation

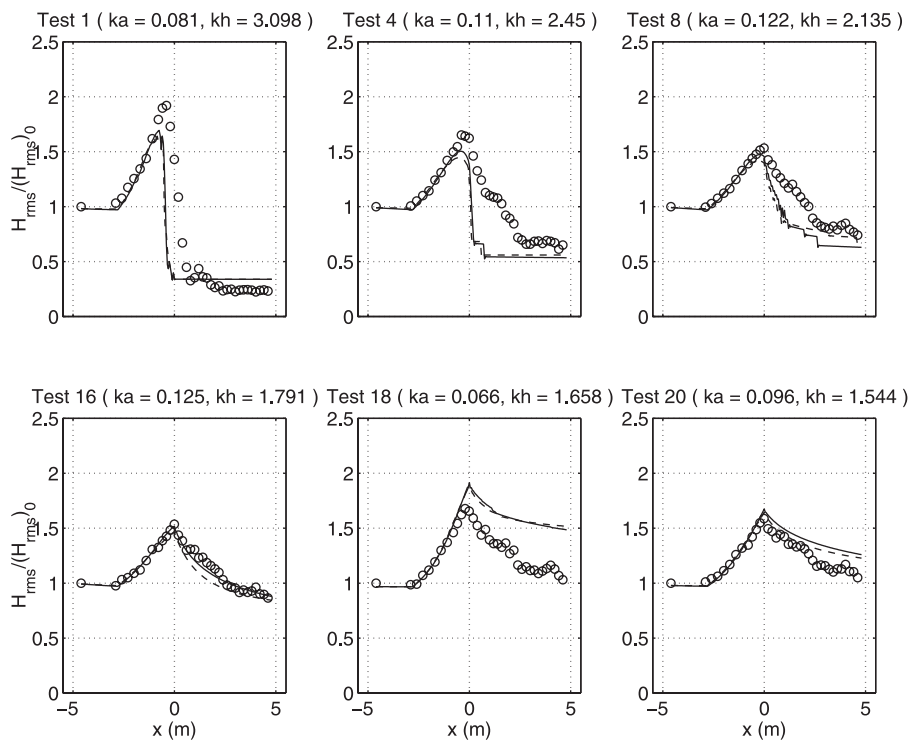


Figure 21. Normalized H_{rms} for representative tests. Solid line shows present dissipation model; dashed line shows the *Battjes and Janssen* [1978] dissipation model; and circles show data. Initial wave steepness ka is given within brackets.

given by equation (29). Hence the breaking parameter β must be calibrated to a larger value. The effect of the downshift in $\bar{\omega}$ can be seen in the comparisons of the spectral model and the bulk conservation model in Figure 17. Both models use the same dissipation formulation given by equation (29). However, while the spectral model shows some capability in simulating the downshift in $\bar{\omega}$, the bulk conservation model is unable to do so (see Figure 18). As a result, in the test cases where the bulk conservation model can propagate energy through the channel (tests 16, 18, and 20), the energy dissipation is much greater in the bulk conservation model than in the spectral model.

6. Conclusions

[50] A series of experiments for both monochromatic and random waves have been conducted to study energy dissipation due to wave breaking under conditions of strong opposing currents. Comparison with data has shown that a modified bore dissipation model works very well. The modified model uses a wave slope criterion instead of the standard wave height to water depth ratio that is used for shallow water breaking. The *Battjes and Janssen* [1978] model, which also uses a wave slope criterion to determine breaking, compares very well with the data also. Due to the significant steepening of the waves, nonlinear terms in the dispersion relation become important and must be accounted for in numerical models. Under certain conditions the development of sideband instabilities can play a crucial role in the dynamics of the wave field close to the blocking region. As random waves propagate into stronger opposing currents, the frequency spectrum downshifts considerably due to the blocking of higher frequency components. This downshift can be modeled with a spectral model. The spectral model does not account for frequency downshifting due to wave modulation, which is a nonlinear process.

[51] Unlike the depth-limited breaking tests the parameters quantifying energy dissipation in current-limited breaking have different values for monochromatic and random wave tests. This is partly due to the nonmonotonic nature of the opposing current in our experiments and partly due to the dependence of the dissipation formula on the wave steepness. In the random wave tests the spectrum wave steepness is quantified by a bulk spectral quantity $\bar{\omega}$, which downshifts due to both nonlinear effects and blocking of the higher frequency parts of the spectrum. This results in smaller estimates of energy dissipation from the bulk dissipation formula and leads to higher values for the calibrating parameter. In the monochromatic tests, downshift in wave steepness is achieved only due to nonlinear effects.

[52] The advantage of using equations (12) and (29) to simulate current-limited wave breaking is that in shallow water they reduce to their corresponding forms used in depth-limited breaking. It should be kept in mind though that depth-limited breaking is very different from current-limited breaking, as is shown by the different values of the parameters β and γ in the two cases. It will be useful to have the parameters as a function of current and water depth, so

that a breaking model can be used in a range of different conditions.

[53] **Acknowledgments.** This research has been sponsored by the NOAA Office of Sea Grant, Department of Commerce, under grant NA56RG0147 (project R/OE-21). The U.S. Government is authorized to produce and distribute reprints for governmental purposes, notwithstanding any copyright notation that may appear herein.

References

- Badulin, S. I., K. V. Pokazayev, and A. D. Rozenberg, A laboratory study of the transformation of regular gravity-capillary waves in inhomogeneous flows, *Izv. Atmos. Ocean. Phys.*, 19(10), 782–787, 1983.
- Battjes, J. A., and J. P. F. M. Janssen, Energy loss and set-up due to breaking of random waves, *Proc. Int. Conf. Coastal Eng.* 16th, H569–H587, 1978.
- Benjamin, T. B., and J. E. Feir, The disintegration of water waves on deep water, 1, Theory, *J. Fluid Mech.*, 27, 417–430, 1967.
- Bouws, E., H. Gunther, W. Rosenthal, and C. L. Vincent, Similarity of the wind wave spectrum in finite depth water, *J. Geophys. Res.*, 90, 975–986, 1985.
- Bretherton, F. P., and C. J. R. Garrett, Wavetrains in inhomogeneous moving media, *Proc. R. Soc. London, Ser. A.*, 302, 529–554, 1969.
- Chawla, A., and J. T. Kirby, Experimental study of wave breaking and blocking on opposing currents, *Proc. Int. Conf. Coastal Eng.* 26th, 759–772, 1998.
- Chawla, A., and J. T. Kirby, Waves on opposing currents: Data report, *Tech. Rep. CACR-99-03*, Cent. for Appl. Coastal Res., Univ. of Delaware, Newark, Del., 1999.
- Hasselmann, K., On the spectral dissipation of ocean waves due to white-capping, *Boundary-Layer Meteorol.*, 6, 107–127, 1974.
- Lai, R. J., S. R. Long, and N. E. Huang, Laboratory studies of wave-current interaction: Kinematics of the strong interaction, *J. Geophys. Res.*, 94, 16,201–16,214, 1989.
- LeMéhauté, B., On non-saturated breakers and the wave run-up, *Proc. Int. Conf. Coastal Eng.* 8th, 77–92, 1962.
- Longuet-Higgins, M. S., and M. H. Fox, Theory of the almost-highest wave: The inner solution, *J. Fluid Mech.*, 80, 721–741, 1977.
- Longuet-Higgins, M. S., and N. D. Smith, Measurement of breaking waves by a surface jump meter, *J. Geophys. Res.*, 88, 9823–9831, 1983.
- Peregrine, D. H., Interaction of water waves and currents, *Adv. Appl. Mech.*, 16, 9–117, 1976.
- Pokazayev, K. V., and A. D. Rozenberg, Laboratory studies of regular gravity-capillary waves in currents, *Oceanology*, 23(4), 429–435, 1983.
- Ris, R. C., and L. H. Holthuijsen, Spectral modeling of current induced wave-blocking, *Proc. Int. Conf. Coastal Eng.* 25th, 1246–1254, 1996.
- Shyu, J. H., and O. M. Phillips, The blockage of gravity and capillary waves by longer waves and currents, *J. Fluid Mech.*, 217, 115–141, 1990.
- Shyu, J. H., and C. C. Tung, Reflection of oblique waves by currents: Analytical solutions and their application to numerical computations, *J. Fluid Mech.*, 396, 143–182, 1999.
- Smith, R., Reflection of short gravity waves on a non-uniform current, *Math. Proc. Cambridge Philos. Soc.*, 78, 517–525, 1975.
- Thornton, E. B., and R. T. Guza, Transformation of wave height distribution, *J. Geophys. Res.*, 88, 5925–5938, 1983.
- Trulsen, K., and K. B. Dysthe, Frequency down-shift through self modulation and breaking, in *Water Wave Kinematics*, edited by A. Torum and O. T. Gudmestad, pp. 561–572, Kluwer Acad., Norwell, Mass., 1990.
- Trulsen, K., and C. C. Mei, Double reflection of capillary/gravity waves by a non-uniform current: A boundary-layer theory, *J. Fluid Mech.*, 251, 239–271, 1993.
- Xu, D., P. A. Hwang, and J. Wu, Breaking of wind-generated waves, *J. Phys. Oceanogr.*, 16, 2172–2178, 1986.

A. Chawla, Center for Coastal and Land-Margin Research, Department of Environmental Science and Engineering, Oregon Graduate Institute of Science and Technology, P.O. Box 91000, Portland, OR 97291-1000, USA. (arun@ccalmr.ogi.edu)

J. T. Kirby, Center for Applied Coastal Research, University of Delaware, Newark, DE 19716, USA. (kirby@udel.edu)